Zigzag slabs for solid-state laser amplifiers: batch fabrication and parasitic oscillation suppression

Arun Kumar Sridharan, Shailendhar Saraf, Supriyo Sinha, and Robert L. Byer

We have developed a 100 W class Nd:YAG master oscillator power amplifier system based in part on an end-pumped zigzag slab power amplifier. This amplifier incorporates parasitic oscillation suppression by using roughened edges and achieves a small-signal gain coefficient ($g_0 l$) of 8.06. We describe a novel technique for suppression of parasitic oscillations using claddings on slab edges that significantly increases $g_0 l$ to 11.63 and increases the single-pass extracted power in a power amplifier by 50%. Commercial use of these zigzag slab amplifiers has been limited by the time and cost of production. We describe a new batch fabrication technique that improves the quality and significantly reduces the cost of zigzag slabs.

OCIS codes: 140.3280, 140.3350.

1. Introduction

Applications such as gravitational-wave detection require high-average-power laser sources with a high degree of spectral and spatial coherence. For example, the proposed Advanced Laser Interferometer Gravitational Wave Observatory (LIGO) requires a 200 W, single-longitudinal-mode, single-transverse-mode Nd:YAG laser as compared with the 10 W laser used continually on site since 1997.[1,2] Several approaches to meet this requirement are being investigated. Traditional rod-based injection-locked lasers operate at 114 W.[3] Thermal lensing and stress-induced birefringence present challenges to their power scaling. Large-core double-clad fiber amplifier-based sources have reached 264 W of output power.[4] However, their phase noise, pointing stability, and long-term reliability have to be characterized with respect to the demanding LIGO requirements. We have investigated a master oscillator power amplifier (MOPA) approach based on end-pumped zigzag slab amplifiers to take advantage of the well-known power scaling of slab lasers and the reliability and coherence-preserving properties of power amplification.

In addition to scientific applications, commercial applications also motivate several approaches for scaling solid-state lasers to high average powers. For example, active mirror slab lasers also known as thin-disk lasers, first invented by Martin and Chernoch[5] and extensively developed by Giesen and colleagues,[6,7] have reached the 1 kW class in multiple transverse modes. Power scaling is difficult because of their one-sided cooling and the practical aspects to operate at a thickness below 100 μm. The zigzag, rectilinear geometry, slab-based[5] MOPA system can scale to higher average powers while maintaining a high beam quality. The slab lasers are cooled symmetrically on both sides and their average power output scales with the cooled area. The nearly one-dimensional thermal gradients and the zigzag optical path of slab laser gain media significantly reduce thermal lensing and stress-induced birefringence compared with traditional rod-based designs.[8,9]

Early zigzag slab laser designs had low efficiencies due to flashlamp pumping. Residual phase distortions and a complex direct water-cooled laser head added to the engineering challenges.[10] Most of these engineering problems have now been solved by laser diode pumping through the end[11] and edge[12] of conduction-cooled zigzag slabs.[13] Nd:YAG zigzag slab lasers now operate at multikilowatt output powers with good beam quality.[14]

Motivated by LIGO, we have developed a Nd:YAG laser in a MOPA configuration. By incorporating the innovations of conduction cooling, edge pumping, and end pumping we have developed a 104 W single-frequency, single-mode, single-polarization Nd:YAG

The authors are with the Edward L. Ginzton Laboratory, Stanford University, Stanford, California 94305. A. K. Sridharan's e-mail address is aruns@stanford.edu.

Received 30 September 2005; accepted 30 October 2005; posted 21 December 2005 (Doc. ID 65087).

0003-6935/06/143340-12$15.00/0

MOPA at 1064 nm using four stages of amplification.[15] An end-pumped zigzag slab power amplifier forms the final stage and accepts a 30 W input signal beam. It is double passed and operates at 104 W with an M^2 of 1.08 and 1.13 in the zigzag and nonzigzag directions, respectively. To determine the spatial coherence of this system, the MOPA output is mode matched into a Fabry–Perot ring resonator called a mode cleaner,[16] which resonates the TEM_{00} Gaussian mode. We determined that 89% of the 104 W output signal is in the fundamental TEM_{00} spatial mode, and its degree of polarization is greater than 97%. These results along with quantum noise measurements in an end-pumped, saturated, zigzag Nd:YAG slab amplifier[17] are key milestones in the development of a 200 W laser system for the next-generation Advanced LIGO system.

In this paper we focus on the design, fabrication, and performance of the end-pumped zigzag slab power amplifier. To achieve power scaling in the MOPA configuration, the power amplifier must be designed to allow efficient power extraction. The output intensity of a solid-state power amplifier is given by[18]

$$I_{\text{out}} = I_{\text{in}} \exp\left[g_0 l \left(1 + \frac{I_{\text{in}}}{I_{\text{sat}}}\right)^{-1}\right], \tag{1}$$

where I_{out} is the output intensity, I_{in} is the input signal intensity, g_0 is the small-signal gain coefficient, l is the signal optical path length, and I_{sat} is the saturation intensity of the gain medium. A high $g_0 l$ and $I_{\text{in}} > 2I_{\text{sat}}$ is needed to extract >97% of the available power from a power amplifier. In practice, either parasitic oscillations or amplified spontaneous emission (ASE) clamps $g_0 l$ and thereby limits the extraction efficiency. We present a novel technique that involves application of claddings on the zigzag slab's non-total-internal-reflection surfaces (edges) to increase the parasitic-limited $g_0 l$ and extracted power in a saturated amplifier.

Model calculations show that $g_0 l > 7$ and a cross-sectional area of 1 mm^2 per slab is required to extract 170 W of power and achieve 200 W output with an available 30 W of input power in two end-pumped zigzag slab amplifier stages. To achieve efficient power extraction from the amplifier in a TEM_{00} Gaussian mode, we chose an approximately 1:1 (width:thickness = 1.1:0.9 mm) aspect ratio slab.

Fabrication of a high length-to-thickness aspect ratio, slab (1.1 mm × 0.9 mm × 66 mm, doped region with undoped end caps) presents challenges. Slabs fabricated individually are of lower quality (surface flatness and coating properties are not uniform) and higher cost (ten times higher) than slabs made by the batch fabrication process presented in this paper. By necessity, we developed a cost-effective way for making zigzag slabs that involves fabricating multiple slabs in batch processing steps. This technique also enables production of higher-quality slabs for optimum amplifier performance. A key side benefit of this invention is that it provides a multiplicity of slabs for testing various parasitic oscillation suppression techniques for improved amplifier power extraction.

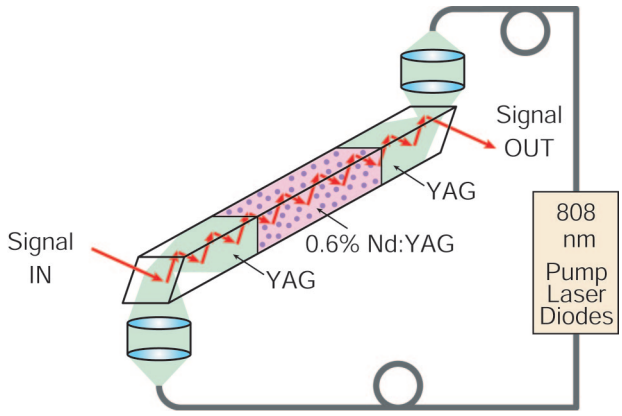

Fig. 1. Diagram of the end-pumped Nd:YAG slab amplifier.

2. Theory, Design, and Modeling

Figure 1 shows a diagram of the end-pumped Nd:YAG zigzag slab amplifier. The amplifier slab is pumped by fiber-coupled laser diodes and reimaged with a lens into the end of the slab. The slab consists of a doped region diffusion bonded to undoped end caps. The pump light undergoes total internal reflection (TIR) at the slanted undoped endface of the slab, is confined by TIR reflections on the four surfaces of the undoped end caps, and is absorbed along the length of the doped region. The length of the doped region is designed to avoid stress fracture and maximize pump absorption, amplifier gain coefficient ($g_0 l$), and power extraction. The signal light is incident at a near-normal angle to the endface and is confined in the slab via TIR reflections on the top and bottom (side) faces.

A. Theory

First we describe the analytical expressions that govern the performance of the slab amplifier. Zigzag slab laser design was treated earlier by Eggleston *et al.*[8] and recently by Chen *et al.*[19,20] Eggleston *et al.*[21] also extended Franz and Nodvik's amplifier analysis[22] to zigzag slabs that had regions with and without standing waves.

Figure 2 shows the zigzag path in a section of the amplifier slab with regions that do and do not have power extracted by the incident optical beam.

Using the Franz–Nodvik equations[22] and modifying the treatment of Eggleston *et al.*[21] to take into account the less than 100% fill factor in the transverse dimension, the output power P_{out} of the zigzag end-pumped slab single-pass amplifier is given by

$$P_{\text{out}} = I_{\text{sat}} A \cos(\gamma) f(2-f) \times \ln\left(1 + \left\{\exp\left[\frac{P_{\text{in}}}{I_{\text{sat}} A \cos(\gamma) f(2-f)}\right] - 1\right\} \exp(g_0 l)\right), \tag{2}$$

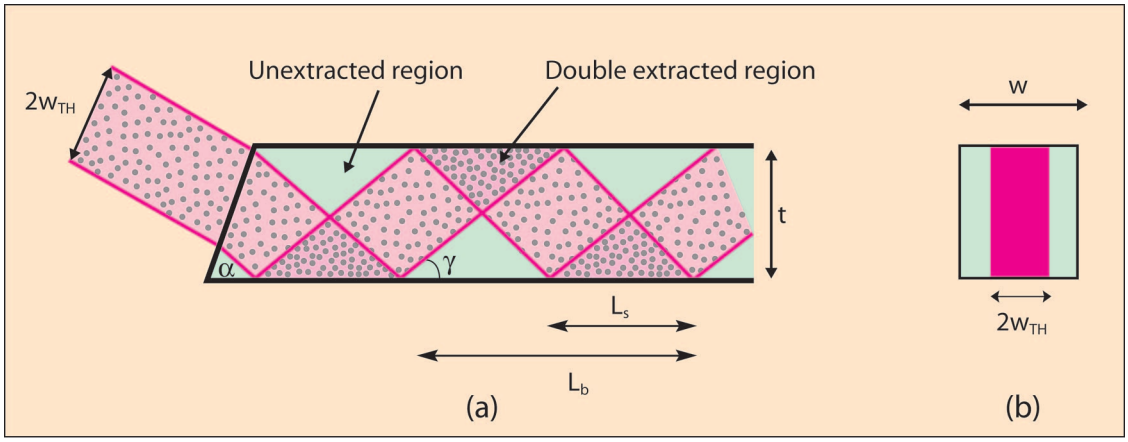

Fig. 2. (a) Geometry of the partially filled slab at near-normal incidence for a single-pass slab amplifier. The bounce period is L_b and the overlap region has a length L_s. (b) The active cross section of the slab has a width of $2w_{\mathrm{TH}}$ and a thickness of t. The active area is partially filled with incident signal power.

where P_{in} is the input signal power and A is the active cross-sectional area of the zigzag slab that is probed by the incident beam and is equal to $2w_{\mathrm{TH}}t$, where w_{TH} is the top-hat equivalent of the TEM_{00} Gaussian beam $1/e^2$ radius w_g in the slab as defined by[18]

$$w_{\mathrm{TH}} = w_g/\sqrt{2}. \tag{3}$$

Here t is the slab thickness and γ is the complementary angle to the angle of incidence at the YAG/SiO_2 interface. The overlap factor f for near-normal incidence in a zigzag slab can be calculated by trigonometry and is given as

$$f = \frac{L_s}{L_b} = \frac{1}{\sqrt{2}}\frac{w_g}{t}\sec\gamma, \tag{4}$$

where L_s is the overlap length given by

$$L_s = \sqrt{2}\,\frac{w_g}{\sin\gamma}, \tag{5}$$

and L_b is the bounce length given by

$$L_b = \frac{2t}{\tan\gamma}. \tag{6}$$

The small-signal gain coefficient $g_0 l$ is given by

$$g_0 l = \frac{P_{\mathrm{pump}}\eta}{wtI_{\mathrm{sat}}\cos\gamma}, \tag{7}$$

where P_{pump} is the incident pump power and η is a pump efficiency factor given by

$$\eta = \eta_{\mathrm{abs}}\eta_p\eta_q. \tag{8}$$

Here the pump absorption efficiency η_{abs} is given as

$$\eta_{\mathrm{abs}} = [1 - \exp(-\kappa l_{\mathrm{doped}})]\eta_c, \tag{9}$$

where η_c is the confinement efficiency of the pump light in the slab, $\kappa = 1.8\ \mathrm{cm}^{-1}$ is the pump absorption coefficient for 0.6% Nd:YAG at 808 nm, and l_{doped} is the length of the slab's doped region. $\eta_p = 0.92$ is the approximate pump quantum efficiency for 0.6% Nd:YAG,[23] and $\eta_q = 0.76$ is the quantum defect given by the ratio of signal and pump photon energies.

To model the power extraction from a power amplifier, the available power in the active cross section of this slab power amplifier is given by

$$P_{\mathrm{avail}} = P_{\mathrm{pump}}\eta\,\frac{A}{wt}. \tag{10}$$

The maximum extractable power P_{extr} for a zigzag optical path is given as[21]

$$P_{\mathrm{extr}} = P_{\mathrm{avail}}\,f(2-f). \tag{11}$$

The unextracted power $P_{\mathrm{unextracted}}$ in the active area due to the zigzag optical path is given by[21]

$$P_{\mathrm{unextracted}} = P_{\mathrm{avail}}(1-f)^2. \tag{12}$$

B. Design

Using these relations, we design the slab amplifier to achieve ~100 W of output power with 30 W of input power and 430 W of pump power. The signal beam must enter and exit the slab without degradation in beam quality due to diffraction losses at the endfaces. The length of the doped region is chosen to achieve full absorption of the pump radiation and a sufficiently cooled area to avoid stress fracture. The undoped crystal length must be long enough to prevent clipping of the pump radiation as it is focused onto the slab's endfaces, adjacent to the copper microchannel coolers.

Figure 3(a) depicts the slab dimensions as well as the properties of the coatings on the end and TIR

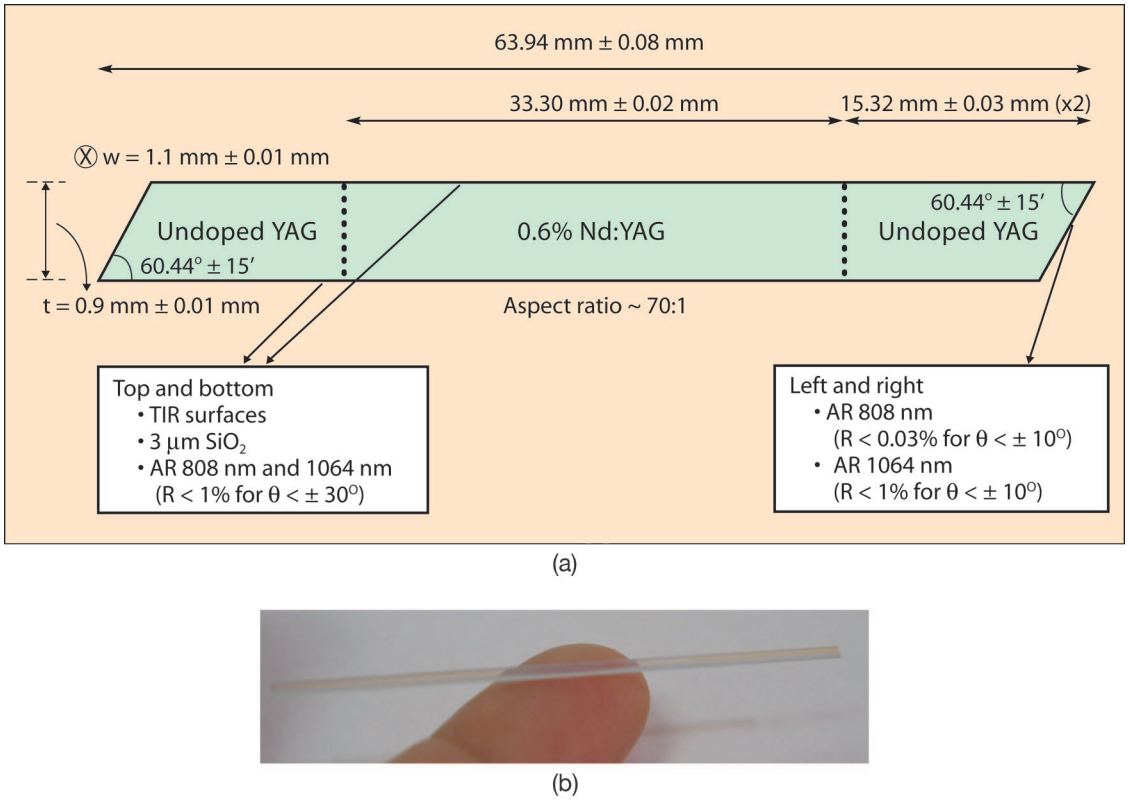

Fig. 3. (Color online) (a) Two-dimensional view of the slab with dimensions and coating properties. (b) Photograph of a fabricated Nd:YAG slab.

surfaces. The required slab cross-sectional area is 1 mm^2. To achieve efficient power extraction from the amplifier in a TEM_{00} Gaussian mode, we choose an approximately 1:1 (w:t = 1.1:0.9 mm) aspect ratio slab.

The slab is conduction cooled on the top and bottom faces. A 3 μm thick SiO_2 coating deposited on these surfaces ensures TIR zigzag reflections for the signal beam with minimum loss by allowing the evanescent wave to be attenuated. The net loss for the signal beam due to residual scattering at the YAG/SiO_2 interface is less than 0.1%/bounce. A thin indium film thermal layer followed by copper microchannel coolers[24] is placed in contact with the SiO_2 layer to extract the heat deposited under operating conditions in the slab.

In our implementation, the 3 μm thick SiO_2 coatings provide improved optical performance in two distinct and independent ways. The first function is to achieve an antireflection (AR) coating for light at the pump wavelength λ_p at $\theta < 30°$ (θ is defined as the angle with respect to the normal vector for each surface). This coating design reduces losses when optical end pumping is performed through the TIR surfaces as shown in Fig. 1. The second function is to suppress parasitic oscillations by increasing the loss for spontaneous emission or ASE rays that are incident on the TIR surfaces at less than the critical angle (θ_{crit}). This is achieved by embedding an AR coating at the laser wavelength λ_s within the SiO_2 layer. This coating has a power reflectivity R less than 1% for rays that are incident on the TIR surfaces from within the slab at angles less than $\sim 0.9\ \theta_{crit}$. θ_{crit} for a YAG/SiO_2 interface is 52.8°, whereas for a YAG/air interface it is 33.2°. The coating allows more ASE rays to refract out of the slab and into the SiO_2 coating layer and eventually be absorbed in the indium thermal layer or copper microchannel cooler that is in contact with this coating layer.

An AR coating is also deposited on each of the end-coupling faces of the slab. This coating is a multilayer AR coating at λ_p and λ_s. The coating enables an alternative for efficient pumping of slabs via the end-coupling faces and ensures minimal loss to the amplified signal beam, respectively. The edge faces are polished at the end of fabrication.

Fabricating a high length-to-width aspect ratio Nd:YAG slabs individually is difficult. Slabs made individually are of lower quality with respect to surface flatness and nonuniform coating properties. We therefore developed a mass fabrication technique that produced multiple slabs but involved intermediate polishing and coating steps that utilized large surface areas. The steps include bonding undoped YAG to either side of a doped YAG block to form a sandwich, and dicing the sandwich to provide slices. Two of the surfaces of each slice are cut, ground, and polished as TIR surfaces. The slices' end surfaces and the TIR surfaces are appropriately coated. Finally, the coated slice is diced perpendicular to the TIR

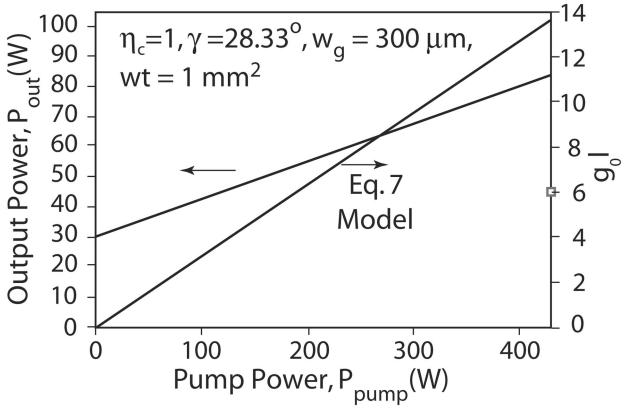

Fig. 4. Expected amplifier gain coefficient ($g_0 l$) and single-pass output power P_{out} (W) versus pump power P_{pump} (W). $\eta_c = 1$, $\eta_{abs} = 1$, $\eta_q = 0.76$, $\eta_p = 0.92$, $\gamma = 28.33°$, $f = 0.26$, $w_g = 300$ μm, $wt = 1$ mm^2, $I_{sat} = 2500$ kW/cm^2, $P_{in} = 30$ W.

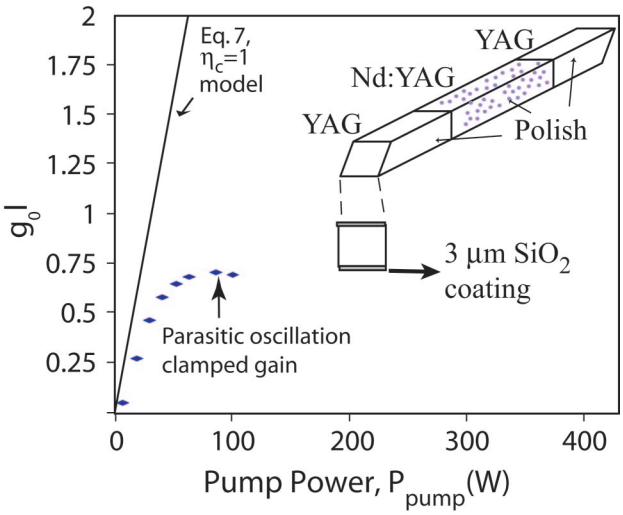

Fig. 5. (Color online) Schematic of the fabricated slab with polished non-TIR (edge) faces and the small-signal gain versus pump power P_{pump} (W).

surfaces and the edges are polished to provide many zigzag slabs at reduced cost. Appendix A describes in detail how the slab described above [Fig. 3(b)] is fabricated and the related cost-benefit analysis.

C. Modeling

Using Eqs. (2)–(8), we model the expected performance of the Nd:YAG end-pumped zigzag slab amplifier. The initial goal is to achieve >100 W of output signal power with 430 W of available pump power and 30 W of input signal power.

Figure 4 shows the expected output power and $g_0 l$ of a slab amplifier whose cross-sectional area ($w \times t$) is determined by iterating on the slab length, apex angle α, bounce angle γ, signal mode size w_g, and solving Eqs. (2)–(9) to achieve ~83 W of single-pass output power (input power plus extracted power). Using Eq. (12) we calculate that the unextracted power in the active area $P_{unextracted}$ is 62.4 W. To achieve additional power extraction on the second pass from this heavily saturated amplifier, it is essential that the single-pass output signal be angular multiplexed[25] to extract from unprobed regions within the active area. On the basis of practical experience, we expect that half of the single-pass unextracted power $P_{unextracted}$ can be extracted on the second pass. This yields an estimated double-pass output of 117 W. The values selected for the end-pumped Nd:YAG zigzag slab amplifier are $\eta_c = 1$, $\eta_{abs} = 1$, $\eta_q = 0.76$, $\eta_p = 0.92$, $I_{sat} = 2500$ kW/cm^2, $\gamma = 28.3°$, $f = 0.26$, $w_g = 300$ μm, and $wt = 1$ mm^2.

For these values, the model predicts a small-signal gain coefficient $g_0 l$ of 13.57 at 430 W of pump power. At this gain level, the calculated single-pass output power is 83 W and the estimated double-pass output exceeds 100 W.

3. Performance

We tested the performance of the Nd:YAG slab amplifier by pumping each end with up to 215 W of 808 nm laser diode power. We used a 1 mW, 1.064 μm probe beam to measure the small-signal gain coefficient of the slab.

Figure 5 depicts the gain coefficient versus pump power for the fabricated slab with polished edges. Visual inspection of the polished side faces of the slab under pumping conditions confirms the expected nearly 100% pump confinement efficiency ($\eta_c \approx 1$).

Figure 5 shows that the $g_0 l$ of this slab amplifier is clamped even at low pump powers and is pinned at 0.7 at 80 W of pump power due to parasitic oscillations. The all-sides-polished slab provides high reflectivity from the surfaces and permits parasitics to clamp the gain. Since the extracted power in a saturated amplifier is proportional to $g_0 l$ this amplifier slab is unsuitable for efficient power extraction. We next focus on ways to increase the gain of the fabricated slab by suppressing parasitic oscillations.

4. Parasitic Oscillation Suppression

A. Background

A parasitic oscillation is basically a laser oscillator with a threshold dependent on optical path losses. The simplest parasitic oscillation occurs when the slab itself forms the cavity. The small-signal gain coefficient $(g_0 l)_{parasitic}$ at parasitic oscillation threshold is defined by

$$(g_0 l)_{parasitic} = -\frac{1}{l_T} \ln\left(\prod_{i=1}^{N} R_i\right), \tag{13}$$

where R_i is the parasitic loop's ith reflection coefficient and l_T is the parasitic loop's total path length.[27] To maximize $(g_0 l)_{parasitic}$, the reflection coefficient from each slab surface should be minimized or efforts should be taken to avoid closed optical paths that lower $(g_0 l)_{parasitic}$.

Several techniques have been investigated in the past to minimize the reflection coefficient from the slab

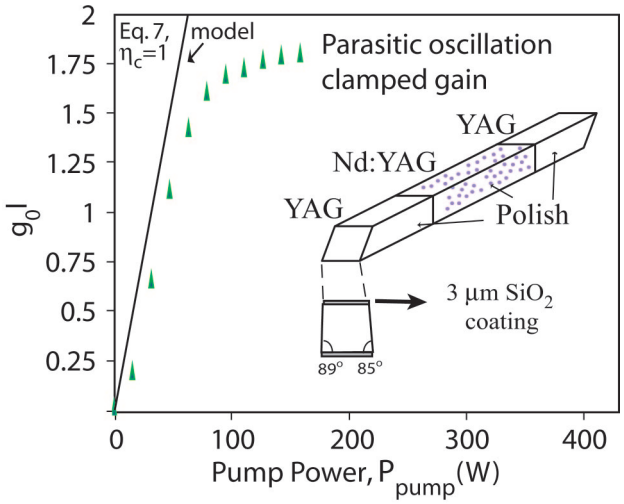

Fig. 6. (Color online) Schematic of polished and beveled side faces of the slab and the small-signal gain ($g_0 l$) versus pump power P_{pump} (W).

surfaces and suppress parasitic oscillations. Rutherford considered the case of two-dimensional transverse parasitic oscillation paths and determined the slab aspect ratio (width:thickness) for which transverse parasitic oscillation paths were suppressed.[28] The problem of identifying parasitic oscillation modes in a three-dimensional slab does not lend itself to analytical treatment. Monte Carlo-based ray-tracing codes have been developed to identify parasitic oscillation paths.[27] Ascertaining the efficacy of various techniques to spoil these parasitic paths is largely based on trial and error. For example, grinding the slab sides to reduce the reflection coefficient is effective, but in addition to leakage of pump radiation, it results in large surface defects that reduce surface strength and lead to premature stress fracture.[29] Using index-matched fluids on the critical surfaces is also effective but requires a more complicated optomechanical laser-head design.[27] Another parasitic suppression technique used in the past involves canting the edge surfaces of the slab. Breaking the symmetry of the slab by beveling the edge faces results in less depletion of the population inversion by the onset of parasitics because they are no longer confined by TIR after successive reflections on the slab surfaces.

We have modified the edge faces of the slab amplifier in three distinct ways to suppress parasitic oscillations. We discuss their relative merits and the resulting improvements in amplifier performance.

B. Method 1: Slabs with Polished and Beveled Edge Faces

Figure 6 depicts our first approach to controlling parasitic oscillations by beveling the edges of the all-sides-polished fabricated slab. Bevels can be incorporated along either the length or the width of the slab. Bevels along the length in a 66 mm long slab are impractical because a significant amount of aperture is lost on the endfaces. We implemented transverse

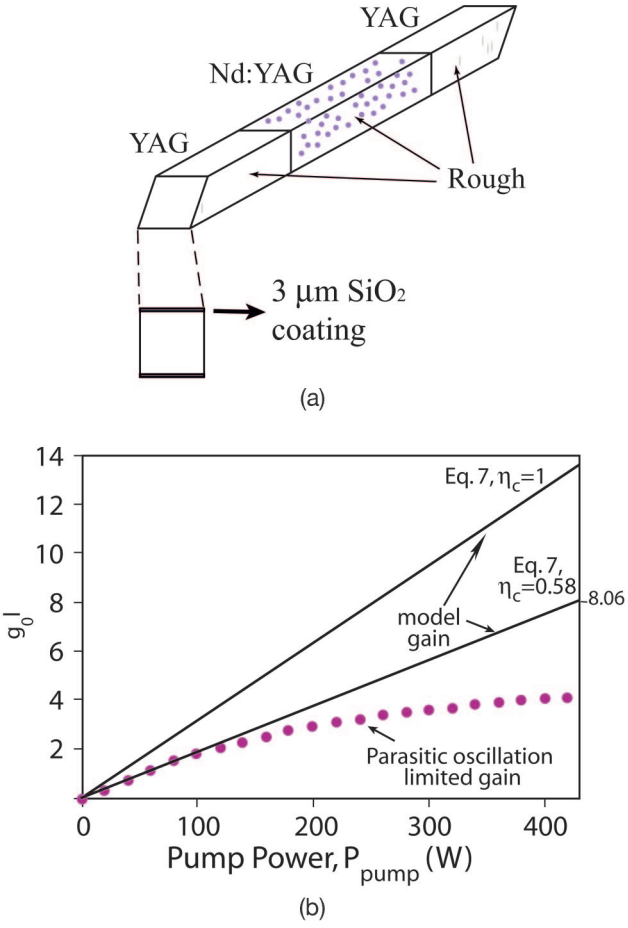

Fig. 7. (Color online) (a) Schematic of rough edges of the slab used for parasitic suppression. (b) Parasitic-limited small-signal gain ($g_0 l$) versus pump power P_{pump} (W).

bevels of various angles up to 5° on each face. Transverse bevels of higher angles resulted in marginal parasitic suppression improvement and unacceptable loss of clear aperture for the input signal beam.

Figure 6 shows the small-signal gain performance of an amplifier slab with a 5° bevel on one side face and 1° on the other. The $g_0 l$ of this slab amplifier is saturated even at low pump powers and is pinned at 1.77 at 160 W of pump power due to parasitic oscillations. The small-signal gain performance of this beveled amplifier slab is better than the slab with polished faces whose gain was pinned at 0.7 at 80 W of pump power. Slabs with polished and beveled edges retain the pump confinement and absorption efficiency of a nonbeveled slab amplifier while increasing the parasitic oscillation threshold by 4.6 dB.

C. Method 2: Slabs with Rough Edge Faces

Figure 7(a) depicts our second approach to parasitic suppression that involves roughening the polished edges of the slab by grinding it with 15 μm grit-size aluminum oxide mixed with water on a glass plate. We expect the rough edges to outwardly scatter light and increase the parasitic oscillation threshold.

Figure 7(b) shows the small-signal gain perfor-

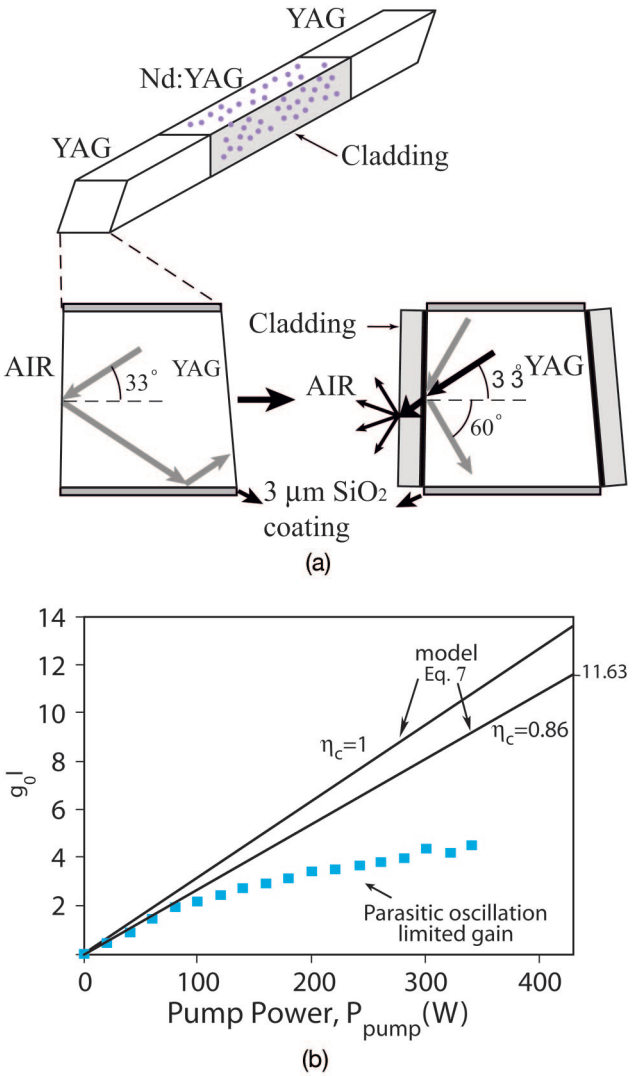

Fig. 8. (Color online) (a) Illustration of slabs with claddings on edges for parasitic suppression. (b) Parasitic-limited small-signal gain ($g_0 l$) versus pump power P_{pump} (W).

mance of this slab amplifier. The parasitic oscillation-limited $g_0 l$ is increased to 3.9. Visual inspection of the slab during amplifier tests suggested significant pump light loss. To quantify this loss, we draw a line representing the extrapolated small-signal gain. This line represents the gain achievable if parasitic oscillations were negligible. This line can also be derived by using η_c as a fitting parameter and setting it equal to 0.58 in Eq. (7). Thus 42% of the pump light scatters out of the rough edges in the slab.

As the pump power is increased to 430 W, parasitic oscillations saturate the gain below the extrapolated no-parasitic gain limit of 8.06. In a heavily saturated amplifier where $I_{\text{in}} \gg I_{\text{sat}}$, the input beam will outcompete parasitic oscillations, saturate the small-signal gain, and extract power proportional to the no-parasitic $g_0 l$ limit of 8.06 at 430 W of pump power.

The primary drawback of this slab amplifier is the low pump confinement efficiency. The rough edge faces lead to pump light loss but also cause significant outward scatter of parasitic light. Parasitic suppression via polishing and beveling the slab edges results in excellent confinement for pump light and unfortunately for signal parasitic modes as well. Our next approach to parasitic oscillation suppression is a hybrid approach that takes advantage of the pump confinement possible in the polished and beveled slab and the outward-scattering properties of the rough edges slab.

D. Method 3: Slabs with Polished, Beveled, and Cladded Edge Faces

Figure 8(a) shows our novel technique involving a cladding on the edge surfaces to achieve enhanced parasitic suppression. The cladding consists of an optical-grade epoxy that bonds a 100 μm thick piece of silica to YAG. The index of refraction of the cladding, n_{clad}, is selected to transmit the parasitic modes incident on the side faces at $\theta < \theta_{\text{crit}}$ while trapping the pump rays that are incident on the faces at $\theta > \theta_{\text{crit}}$. For a given slab width and thickness, and divergence angle for the pump beam, we calculate the minimum angle θ_{min} at which pump rays are incident on the side faces. θ_{crit} is set just below this value so that all the pump rays are confined due to TIR and absorbed in the doped region. We chose a cladding material such that

$$\theta_{\text{crit}} \cong \sin^{-1}\left(\frac{n_{\text{clad}}}{n_{\text{YAG}}}\right). \tag{14}$$

For our experimental conditions, we chose $\theta_{\text{crit}} = 60°$ and used an optical-grade epoxy with a refractive index of 1.55 as the cladding. To ensure that rays in the cladding do not reenter the slab through TIR at the cladding–air interface, the silica's interface with air is roughened to enable outward scattering.

Figure 8(b) shows the small-signal gain ($g_0 l$) versus pump power P_{pump} (W) in this slab. The small-signal gain coefficient reaches 4.5 at a pump power of 340 W. We use η_c as a fitted parameter, and by setting $\eta_c = 0.86$ in Eq. (7), we find that 14% of pump light scatters out of the cladding in the slab. The extrapolated gain in this slab amplifier without parasitic onset is 11.63 at 430 W of pump power. In a heavily saturated amplifier where $I_{\text{in}} \gg I_{\text{sat}}$, the input beam will extract power proportional to the extrapolated $g_0 l$ of 11.63 at 430 W of pump power.

We summarize the small-signal gain measurements for the slab with rough sides (i.e., original fabricated slab) and the slab with the cladding applied. The extrapolated small-signal gain at a pump power of 430 W is 8.06 for the slab with rough sides, and this improves to 11.63 for the slab with the cladding. The pump absorption efficiency is 58% on the rough edges of the slab and 86% on the slabs with the parasitic suppression cladding. The significantly enhanced small-signal gain in the slab with cladding on the non-TIR faces offers the potential for increased power extraction in a saturated MOPA configuration.

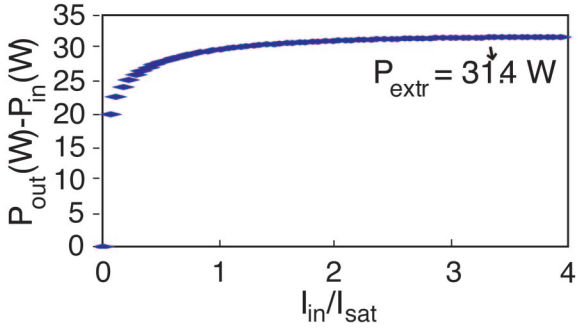

Fig. 9. (Color online) Single-pass extracted power P_{out} (W) − P_{in} (W) versus I_{in}/I_{sat}. Parameters used in Eqs. (2)–(11): w_g = 300 μm, $g_0 l$ = 8.06, γ = 28.33°.

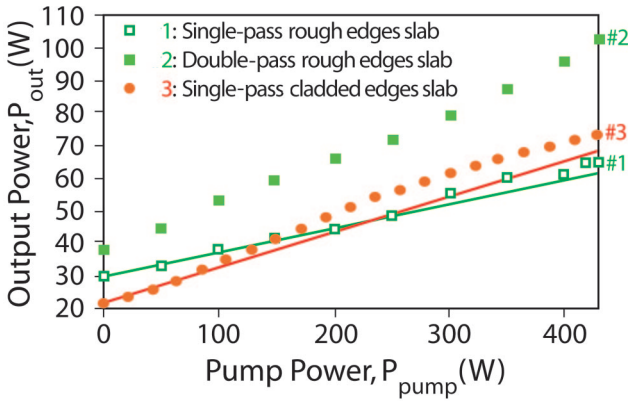

Fig. 10. Total output power versus pump power P_{pump} (W) for the rough and cladded edges of the slabs. The filled circles represent measured values for the three amplifier tests. The solid lines represent the theoretical output power P_{out} (W) expected from Eq. (2) for both single-pass, end-pumped zigzag slab amplifiers. An analytical expression for double-pass output on the rough edges of the slab does not exist.

5. Master Oscillator Power Amplifier Performance

Since the slabs with rough and cladded edges demonstrate the best small-signal gain performance, they are tested as the final stage power amplifier in the Nd:YAG MOPA system. The input signal for this amplifier was the output of the previous amplifier stage. Because of some technical problems, the output of the previous amplifier stage was different when the two different slabs were tested. Regardless, the input signal power focused onto a Gaussian beam spot with w_g = 300 μm $1/e^2$ radius spot size results in $I_{in} > 6I_{sat}$ for amplifier tests on both slabs.

Figure 9 shows the power that is extractable from the rough edges of the slab amplifier as a function of the input intensity normalized to the saturation intensity. Figure 9 is generated by using Eqs. (2)–(9) with the slab dimensions and parameters described in Fig. 3, and setting $g_0 l$ = 8.06, w_g = 300 μm, γ = 28.33°, and I_{sat} at 2.5 kW/cm^2. Figure 9 also shows P_{extr} that is calculated using Eqs. (10) and (11). At a normalized intensity greater than 2, the input signal following a zigzag optical path extracts >97% of the power that is extractable in the active area of the slab (P_{extr}).

This prediction is corroborated by measurements on amplifier extraction based on slabs with rough edges for parasitic suppression. Figure 10 plots the total output power (input power plus extracted power) in the optical beam after the power amplifier for slabs with rough edges and slabs that use claddings for parasitic suppression. The input power is the total output power at P_{pump} = 0. Two fiber-coupled diode lasers requiring ~2.6 kW of electrical power and with total output optical power of 430 W were used for these measurements.

A. Extraction from Rough Edges of the Slab

Figure 10 shows that at the maximum pump power of 430 W, the amplifier with rough edges had a 30 W input and 65 W of single-pass output power (green, open squares) The extracted power is 35 W. The green solid line represents the theoretical output power P_{out} expected from Eq. (2). Using Eqs. (10)–(12) and setting P_{pump} = 430 W and η = 0.41, we calculate that P_{avail} = 68.4 W, P_{extr} = 31.4 W, and $P_{unextracted}$ = 37 W. The 3.6 W discrepancy between the experimental and theoretical values for extractable power is due to a 20 μm measurement uncertainty in the signal spot size (w_g = 300 μm is used in the model). Thus the single-pass, saturated zigzag slab amplifier extracts nearly 100% of the extractable power (P_{extr}) and 51.1% of the power available (P_{avail}) in the active area.

Figure 10 also shows the results of the double-pass end-pumped slab amplifier experiment (green filled squares). To extract power from the slab regions not probed during the first pass, we use angular multiplexing on the second pass.[25] The available signal input power for this experiment is 38 W. By extracting 34 W, the single-pass output is 72 W. To cross the 100 W power level on the second pass, we extract over a larger mode volume by adjusting the signal beam to a measured w_g = 325 μm spot size. The double-pass output power is 104 W and the total extracted power is 66 W. An analytical expression for double-pass output on the rough edges of the slab does not exist. Because the active area is slightly larger for the second pass, we estimate that the net active-area amplifier extraction efficiency is 80%.

B. Extraction from Cladded Edges of the Slab

We next tested the slab with parasitic suppressive cladding on the slab's non-TIR faces. Figure 10 shows that with a 22 W input, this single-pass amplifier yielded 75 W output at 430 W of pump power (red filled circles). The extracted power is 53 W. The red solid line represents the theoretical output power P_{out} expected from Eq. (2). Using Eqs. (10)–(12) and setting P_{pump} = 430 W and η = 0.6, we calculate that P_{avail} = 99.4 W, P_{extr} = 45.6 W, and $P_{unextracted}$ = 53.8 W. The 16% discrepancy between the experimental and theoretical values for extractable power is due to a 20 μm measurement uncertainty in the signal spot size (w_g = 300 μm is used in the model).

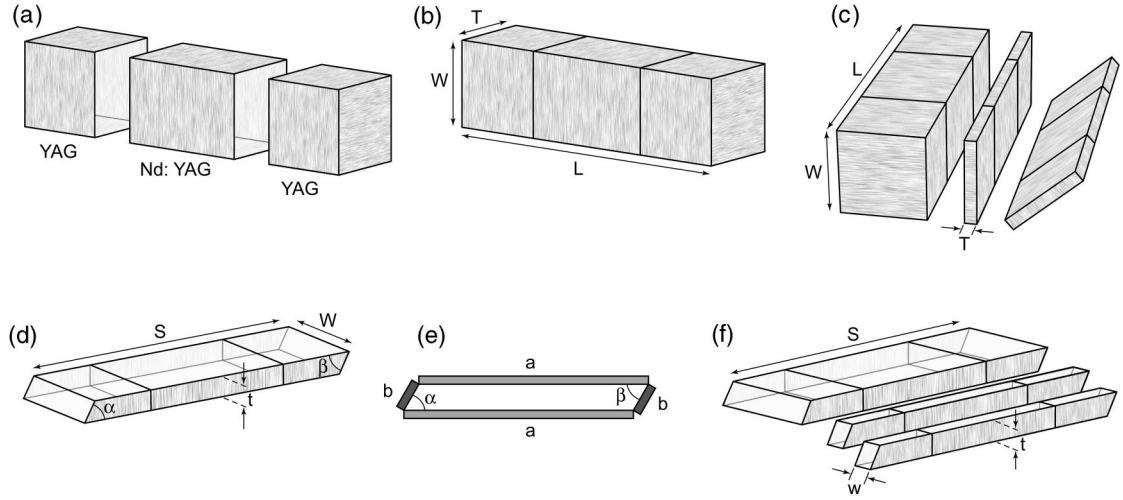

Fig. 11. (a) Schematic of the doped and undoped blocks used to fabricate the zigzag slab. (b) View of a composite block produced from two undoped blocks and one doped block. $W = T = 8$ mm, $L = 70$ mm. (c) Diagram illustrating the dicing of a composite block into plates. (d) Three-dimensional view of a finished slab plate with polished faces and polished ends with angles α and β. The thickness t is the thickness of the final slab. The endface angles and the length S are also the finished dimensions of the slab. (e) Side view illustrating the coatings applied to four sides of the slab slice of (d). (f) Illustration of the dicing of a coated slab plate into completed zigzag slabs.

On the basis of the measurements on the rough edges of the slab amplifier, we expect that double passing this amplifier with $w_g = 300$ μm on the second pass will result in ~25 W of additional extracted power to reach ~98 W output power. The resulting double-pass extraction efficiency of power in the active area is again expected to be approximately 80%.

C. Discussion

At a fixed pump power of 430 W, compared with the rough edges of the slab, we extract an additional 18 W of single-pass output power in the slab with parasitic oscillation suppressive claddings. This represents a nearly 50% increase in the single-pass extracted power. The pump confinement efficiency has similarly increased from 58% to 86%. These are significant improvements over the slab with rough edges. We plan to use this amplifier slab to scale the output power of this system to 200 W.

6. Conclusion

We have developed a 104 W Nd:YAG MOPA system as a step toward meeting the laser requirements for Advanced LIGO. Parasitic oscillations are a key limitation in the development of an efficient power amplifier for this system. We investigated three different methods of parasitic oscillation suppression. Slabs with rough edges have a maximum no-parasitic extrapolated $g_0 l$ of 8.06. We improved this result by incorporating a novel technique involving claddings on the edge faces. Using this technique, a maximum no-parasitic extrapolated $g_0 l$ of 11.63 is achieved at 430 W of pump power. This record gain coefficient resulted in a 50% increase of extracted power from a saturated, single-pass, end-pumped zigzag slab amplifier. The significant improvements in slab amplifier performance using claddings for parasitic suppression are made possible by an accompanying development in the slab fabrication technique. The batch fabrication technique improves the quality and dramatically reduces the complexity and cost of producing zigzag slabs. This advance allowed us to evaluate the effectiveness of various parasitic suppression techniques in a timely and cost-effective way. The combination of parasitic suppression and batch fabrication may enable significantly increased use of zigzag slabs in high-power, solid-state laser and amplifier systems.

Appendix A: Description of Batch Fabrication Method

Figure 11 illustrates the fabrication process. Two undoped YAG blocks are first polished and bonded to opposite faces of a doped Nd:YAG block.

The bonding process must produce an interface of high optical quality between the bonded surfaces. At least three methods are suitable for this purpose, including diffusion bonding,[30] silicate bonding,[31,32] and chemical-activated bonding.[33] We chose diffusion bonding because it was the most commercially mature technology when this project was started. In the diffusion bonding method, the bonding surfaces are first polished flat to within $\lambda/10$ and cleaned. They are then joined together to make one composite structure. This assembly is heated to a temperature close to the melting point of the host material. Interdiffusion of material at the two interfaces causes bonding between the mated surfaces. One of the advantages of diffusion bonding is that no glues or other agents are required, which increases the optical damage threshold. This method requires heat treatment of the laser material at temperatures in excess of 1000 °C for many hours, much more than what is required with other bonding techniques. In our experience, this step is key to achieving a bond that withstands high thermal stress during laser operation.

Figure 11(b) shows the composite block following the diffusion bonding step. The composite block has the length L, width W, and thickness T required for producing the desired number of zigzag slabs. For the amplifiers developed in this work, the blocks were 8 mm × 8 mm on the sides with a total composite length L of 70 mm.

Next, the interfaces delimiting the doped and undoped regions of the slab sandwich are visually inspected to ensure that they are free of defects. To ascertain whether the composite block can withstand the stresses induced during further fabrication steps, a bond strength test is especially useful. The strength of the bond also gives an indication of the amount of thermal stress the finished slab can withstand during laser operation. A shear strength test can be applied to evaluate the force required to break the bond. We unfortunately did not perform shear strength tests on the Nd:YAG composite blocks but instead had strength tests performed commercially on similarly fabricated Yb:YAG slab plates. These plates, similar to the Nd:YAG plates shown in Fig. 11(d), were 11 mm × 5 mm × 0.4 mm. The test setup involves an Imada DPS-110 load cell on an Imada test stand with a custom clamping mechanism. The tests showed that diffusion-bonded Yb:YAG plates fractured in the bulk with a 2.2 kg mass object exerting pressure over a 2 mm × 2 mm area on the plates' large surfaces. Since the block did not break at the bond interface, we infer that the diffusion-bonded blocks are mechanically as strong as bulk YAG. We did not perform further tests on diffusion-bonded blocks as diffusion-bonded (produced by Onyx Optics) slab lasers had been commercially operated at the 400 W pump power levels.[11]

Figure 11(c) illustrates the next step in which the slab sandwich is sliced perpendicular to its thickness to produce a number of slab plates with thickness t. This step creates multiple minute fractures in the slab plates, which leads to undesirable reduction in the fracture resistance. However, the residual microcracks can be removed by taking off ~150 μm of material from the plate while grinding and polishing. At the end of this polishing step, the two large surfaces of each slab plate are mechanically strong and have a flatness of $\lambda/10$ to ensure TIR with minimal distortion of the beam phase front. The variation in thickness t should be less than 0.01 mm to prevent clipping of the zigzagging signal beam at the output endface.

Next, the faces at both ends of each slab plate are polished at an angle to enable coupling of the signal beam into the zigzag slab and the pump radiation through TIR. Figure 11(d) shows plates with an apex angle α at one end and β at the other end. The angles' values are chosen after careful simulation of the propagation of the pump and signal beams through the slab. During this processing step care must be taken to avoid chips on the end surfaces near the tips, which would increase the chance of catastrophic surface damage under high-power operation. This fabrication step also determines the total length S of the undoped and doped regions. The side cross-sectional view of this slab plate is the same as that of the final zigzag slab.

The finished slab plates are then coated on four surfaces as illustrated in Fig. 11(e). A SiO_2 AR coating is deposited on the plates' large surfaces. They form the TIR surfaces for the finished slabs. The end-coupling faces are AR coated for both λ_s and λ_p wavelengths to minimize loss of the amplified signal as well as to alternatively pump through the endfaces without loss.

Figure 11(f) illustrates the final dicing of a coated slab plate into individual zigzag slabs. The slab plate is diced and polished perpendicular to the TIR surfaces and along the length of the slab. This step defines the width w of each zigzag slab, as well as the surface quality of the sidewalls. The properties of the sidewalls can later be tailored to reduce the possibility of parasitic oscillations. At this point the zigzag slab is ready to be used in a laser or an amplifier.

We began this fabrication process with three composite blocks that were diced into plates, polished, coated, and finally diced to achieve the final slab dimensions. These plates were then finally diced to produce the finished slabs. By starting with an 8 mm × 8 mm × 70 mm bonded block, we were able to fabricate 30 slabs. We optically tested ~10 slab amplifiers and they performed identically. We believe this performance will be maintained as the fabrication process is scaled up to produce more slabs. Another advantage of this fabrication process stems from the fact that most of the intermediate steps involved working with material that had large surface areas. This fact resulted in mechanically stronger diffusion-bonded blocks, the surface quality (i.e., flatness and parallelism requirements) of the polished surfaces was better controlled, and the reflectivity of the coatings was more uniform across the surfaces.

The polishing and dicing were performed by one commercial vendor and the coating operations by another. Both vendors needed to machine special tools that held the slab plates while they were being diced, polished, and coated. Because these tools were tiny (i.e., <1 mm critical dimensions), their machining required special expertise and resulted in higher than average manufacturing costs. The coating steps were also delicate operations because, while one of the surfaces was being coated, all the others needed to be lithographically masked. This was done to ensure that there was no spillover of coating compounds meant for one surface onto a surface that is designed to have completely different optical properties. Table 1 summarizes the fabrication steps and costs.

The cost of each processing step can be divided into nonrecurring and incremental costs. The polishing and coating steps require an initial investment in precision tools in addition to the polishing saw and the coating chamber. When relatively few slabs are fabricated (as is true in our case), Table 1 shows that fixed costs form nearly 50% of the total. However, as the fabrication process is scaled, the fixed costs form

Table 1. Summary of Batch Fabrication Steps and Cost per Operation

Step	Brief Description of the Various Slab Fabrication Steps	Cost ($)	Cost per Slab ($)	Cost per Slab for 1000 Slabs ($)[a]
1	Procure Nd:YAG and YAG raw material and diffusion bond the doped and undoped pieces. The two resultant pieces were 8 mm × 8 mm × 7 cm blocks [Fig. 11(b)].	10,000 Material costs 4620 Bonding cost for two pieces 5380	333	100
2	Perform all dicing and polishing operations to make plates that meet all slab dimension specifications, except for the width. Total of six plates were manufactured [Figs. 11(c) and 11(d)].	17,000 Cost of tools 8500 Cost of dicing and polishing plates 8500	566	100
3	Perform all the coating operations [Fig. 11(e)].	22,500 Cost of tools 11,000 Cost of four coating runs 11,500	750	375
4	Dice and polish the coated slab plates to obtain a multiplicity of slabs having the required width [Fig. 11(f)].	1000	33	25
Total	30 slabs produced	50,500	1682	600

[a]Based on estimates provided by vendors.

a small fraction of the total. Improved efficiencies within the polishing and coating steps result in a much smaller net cost per slab. As Table 1 indicates, the coating step is comparatively more expensive. However, the cost for this step will drop two to three times if 1000 plates are coated. Similarly, improved efficiencies in the other processing steps will result in <$400/slab for truly large-scale manufacturing of slabs.

Finally, it is important to note that fabricating such small slabs would not be possible in a one-by-one fabrication process. Bonding, polishing, and coating such YAG across such tiny dimensions and high length-to-thickness aspect ratios is extremely difficult and prohibitively expensive. As a further illustration of this fabrication process, we have produced Yb:YAG slabs following the above recipe. These slabs (0.4 mm × 0.4 mm × 11 mm, Fig. 12) form the world's smallest slab laser and are useful as pulsed amplifiers for remote sensing applications. This implementation has allowed slab laser devices to scale toward dimensions that were previously only the province of optical fibers.

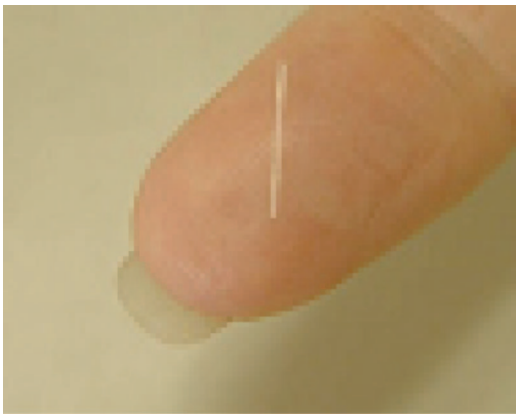

Fig. 12. (Color online) World's smallest Yb:YAG slab laser fabricated by the batch fabrication process (0.4 mm × 0.4 mm × 11 mm).

We have presented a method for batch fabrication of Nd:YAG slabs for use in solid-state lasers. The steps include bonding undoped YAG to either side of a doped YAG block to form a sandwich and dicing the sandwich to provide slices. Two of the surfaces of each slice are cut, ground, and polished as TIR surfaces, then diced perpendicular to the TIR surfaces to provide many zigzag slabs at reduced cost. Thirty slabs were obtained in our implementation of this batch fabrication process. The cost per slab is approximately $1700, which is a small fraction of the overall cost of a typical laser system. By using larger blocks of YAG and Nd:YAG as starter material, and going into mass production (i.e., producing >1000 slabs), the cost per slab can be less than $600. This fabrication procedure can be implemented in almost any crystalline or ceramic host material and dopant(s). A prerequisite is that the material should have the requisite mechanical strength to tolerate the stresses often induced in the slabs during the coating, cutting, and polishing steps. We believe that this slab fabrication process will enable the low-cost manufacture of laser slabs and make them suitable for widespread use in high-power solid-state lasers and amplifiers.

The authors thank Todd Rutherford for helpful discussions in the early phase of this work, Ted Judd of Crystal River Optics for his skill and patience in fabricating numerous slabs, Gary Debell of MLD Technologies for helpful discussions on coating techniques and implementing them, and Karel Urbanek for lots of experimental help in the demonstration of the 100 W MOPA system.[15] This work was supported in part by National Science Foundation grants PHY-0140297 and PHY-9210038 and in part by the U.S. Army Research Office under grant DAAD19-02-1-0184.

References

1. W. Wiechmann, T. J. Kane, D. Haserot, F. Adams, G. Truong, and J. Kmetec, "20 W diode-pumped single-frequency Nd:YAG MOPA for the Laser Interferometer Gravitational Wave Observatory," in *Conference on Lasers and Electro-Optics,* Vol. 6 of OSA Technical Digest Series (Optical Society of America, 1998), p. 432.
2. LIGO II Conceptual Project Book (1999), www.ligo.org/pdf/M990288-A.pdf.
3. M. Frede, R. Wilhelm, M. Brendel, C. Fallnich, F. Seifert, B. Willke, and K. Danzmann, "High power fundamental mode Nd:YAG laser with efficient birefringence compensation," Opt. Express **12,** 3581–3589 (2004).
4. Y. Jeong, J. Nilsson, J. K. Sahu, D. B. S. Soh, C. Alegria, P. Dupriez, C. A. Codemard, D. N. Payne, R. Horley, L. M. B. Hickey, L. Wanzcyk, C. E. Chryssou, J. Alvarez-Chavez, and P. W. Turner, "Single-frequency, single-mode, plane-polarized ytterbium-doped fiber master oscillator power amplifier source with 264 W of output power," Opt. Lett. **30,** 459–462 (2005).
5. W. S. Martin and J. P. Chernoch, "Multiple internal reflection face pumped laser," U.S. patent 3,633,126 (4 January 1972).
6. A. Giesen, H. Hugel, A. Voss, K. Wittig, U. Brauch, and H. Opower, "Scalable concept for diode pumped high power lasers," Appl. Phys. B **58,** 365–372 (1994).
7. C. Stewen, K. Contag, M. Larionov, A. Giesen, and H. Hugel, "A 1-kW cw thin disc laser," IEEE J. Sel. Top. Quantum Electron. **6,** 650–657 (2000).
8. J. M. Eggleston, T. J. Kane, K. Kuhn, J. Unternahrer, and R. L. Byer, "The slab geometry laser. Part 1: Theory," IEEE J. Quantum Electron. **20,** 289–301 (1984).
9. R. J. Shine, Jr., A. J. Alfrey, and R. L. Byer, "40 W CW, TEM_{00}-mode, diode-laser-pumped, Nd:YAG miniature-slab laser," Opt. Lett. **20,** 459–462 (1995).
10. T. Kane, R. Eckardt, and R. Byer, "Reduced thermal focusing and birefringence in zigzag slab geometry crystalline lasers," IEEE J. Quantum Electron. **19,** 1351–1354 (1983).
11. G. D. Goodno, S. Palese, J. Harkenrider, and H. Injeyan, "High average-power Yb:YAG end-pumped zig-zag slab laser," in *Advanced Solid-State Lasers,* C. Marshall, ed., Vol. 50 of OSA Trends in Optics and Photonics Series (Optical Society of America, 2001), pp. 2–4.
12. T. S. Rutherford, W. M. Tulloch, S. Sinha, and R. L. Byer, "Yb:YAG and Nd:YAG edge-pumped slab lasers," Opt. Lett. **26,** 986–989 (2001).
13. A. D. Farinas, E. K. Gustafson, and R. L. Byer, "Design and characterization of a 5.5 W, cw, injection-locked fiber-coupled, laser-diode-pumped Nd:YAG miniature-slab laser," Opt. Lett. **19,** 114–117 (1994).
14. G. D. Goodno, H. Komine, S. J. McNaught, B. Weiss, S. Redmond, W. Long, R. Simpson, E. Cheung, D. Howland, P. Epp, M. Weber, M. McClellan, J. Sollee, and H. Injeyan, "19-kW phase-locked MOPA laser array," in *Advanced Solid-State Photonics*, OSA Trends in Optics and Photonics Series (Optical Society of America, 2006), paper MA2.
15. S. Saraf, S. Sinha, A. K. Sridharan, and R. L. Byer, "100 W, single frequency, low-noise, diffraction-limited beam from an Nd:YAG end-pumped slab MOPA for LIGO," in *Advanced Solid-State Photonics (Nineteenth Topical Meeting and Tabletop Exhibit)*, Postdeadline Proceedings, Vol. 94 of OSA Trends in Optics and Photonics Series (Optical Society of America, 2004).
16. B. Willke, N. Uehara, E. K. Gustafson, R. L. Byer, P. King, S. Seel, and R. L. Savage, Jr., "Spatial and temporal filtering of a 10-W Nd:YAG laser with a Fabry–Perot ring-cavity premode cleaner," Opt. Lett. **23,** 1704–1706 (1998).
17. S. Saraf, K. Urbanek, R. L. Byer, and P. J. King, "Quantum noise measurements in a continuous-wave laser-diode-pumped Nd:YAG saturated amplifier," Opt. Lett. **30,** 1195–1197 (2005).
18. A. E. Siegman, *Lasers* (University Science, 1987).
19. Y. Chen, B. Chen, M. K. R. Patel, A. Kar, and M. Bass, "Calculation of thermal gradient induced stress birefringence in slab lasers. II," IEEE J. Quantum Electron. **40,** 917–927 (2004).
20. Y. Chen, B. Chen, M. K. R. Patel, and M. Bass, "Calculation of thermal gradient induced stress birefringence in slab lasers. I," IEEE J. Quantum Electron. **40,** 909–916 (2004).
21. J. Eggleston, L. M. Frantz, and H. Injeyan, "Derivation of the Franz-Nodvik equation for zig-zag optical path, slab geometry laser amplifiers," IEEE J. Quantum Electron. **25,** 1855–1862 (1989).
22. L. M. Franz and J. S. Nodvik, "Theory of pulse propagation in a laser amplifier," J. Appl. Phys. **34,** 2346–2349 (1963).
23. T. Y. Fan, "Heat generation in Nd:YAG and Yb:YAG," IEEE J. Quantum Electron. **29,** 1457–1459 (1993).
24. J. Fryer, Microcooling Concepts, Inc., 7522 Slater Ave., Suite 122, Huntington Beach, Calif. 92647 (custom design).
25. T. J. Kane and R. L. Byer, "62-dB-gain multiple-pass slab geometry Nd:YAG amplifier," Opt. Lett. **11,** 216–219 (1986).
26. W. Koechner, *Solid-State Laser Engineering,* 5th ed. (Springer-Verlag, 1999).
27. D. C. Brown, D. P. Benfey, W. J. Gehm, D. H. Holmes, and K. K. Lee, "Parasitic oscillations and amplified spontaneous emission in face-pumped total internal reflection lasers," Proc. SPIE **736,** 74–83 (1987).
28. T. Rutherford, "An edge-pumped Yb:YAG laser and phased array resonator," Ph.D. dissertation (Stanford University, 2001).
29. W. F. Krupke, M. D. Shinn, J. E. Marion, J. A. Caird, and S. E. Stokowski, "Spectroscopic, optical, and thermomechanical properties of neodymium- and chromium-doped gadolinium scandium gallium garnets," J. Opt. Soc. Am. B **3,** 102–114 (1986).
30. H. Meissner, "Composites made from single crystal substances," U.S. patent 5,441,803 (15 August 1995).
31. D. Z. Gwo, "Hydroxide-catalyzed bonding," U.S. patent 6,548,176 (15 April 2003).
32. D. Z. Gwo, "Ultra precision and reliable bonding method," U.S. patent 6,284,085 (4 September 2001).
33. N. Traggis, Precision Photonics Corporation, Boulder, Colo. (personal communication, 2005).